SCIENCE CHINA
Earth Sciences

• RESEARCH PAPER •

April 2010 Vol.53 No.4: 575–590
doi: 10.1007/s11430-010-0031-1

# Regional soil moisture simulation for Shaanxi Province using SWAT model validation and trend analysis

LI MingXing[1,2], MA ZhuGuo[1*] & DU JiWen[3]

[1] *Key Laboratory of Regional Climate-Environment Research for Temperate East Asia, Institute of Atmospheric Physics, Chinese Academy of Sciences, Beijing 100029, China;*
[2] *Graduate University of Chinese Academy of Sciences, Beijing 100049, China;*
[3] *Shaanxi Administration of Meteorology, Xi'an 710014, China*

Received February 18, 2009; accepted September 8, 2009; published online March 3, 2010

The soil moisture in Shaanxi Province, a region with complex topography, is simulated using the distributed hydrological model Soil Water Assessment Tool (SWAT). Comparison and contrast of modeled and observed soil moisture show that the SWAT model can reasonably simulate the long-term trend in soil moisture and the spatiotemporal variability of soil moisture in the region. Comparisons to NCEP/NCAR and ERA40 reanalysis of soil moisture show that the trend of variability in soil moisture simulated by SWAT is more consistent with the observed. SWAT model results suggested that high soil moisture in surface soil layers appears in the southern Shaanxi with high vegetation cover, and the Qinling mountainous region with frequent orographic precipitation. In deeper soil layers, high soil moisture appears in the river basins and plains. The regional soil moisture showed a generally decreasing trend on all soil layers from 1951 to 2004, with a stronger and significant decreasing trend in deeper soil layers, especially in the northern parts of the province.

**SWAT, soil moisture content, simulation validation, trend analysis**

**Citation:** Li M X, Ma Z G, Du J W, et al. Regional soil moisture simulation for Shaanxi Province using SWAT model validation and trend analysis. Sci China Earth Sci, 2010, 53: 575−590, doi: 10.1007/s11430-010-0031-1

Soil moisture is one of the key variables in the research of land surface processes. It has significant impacts on climate system and climate change because of its interaction with other components of climate system by mass and energy transfer [1]. The soil moisture governs the processes of evapotranspiration and the water transfer from the soil to the atmosphere. The variations of soil moisture determine the color of the land surface and the growth of the surface vegetation, and thereby influence the optical energy absorption and reflection at land surface [2]. It also can change the thermal capacity of soil, and affect the energy transferring such as latent heat between land surface and the atmosphere. Therefore, understanding the variability of soil moisture can lead us to understand climate system, improve the skills of simulation, and forecast the change of climate. However, the *in situ* observations of soil moisture are short and scarce, which hinders our understanding of the interactions between the soil moisture and the change of climate.

Currently, the research on soil moisture variations focuses on two aspects. One is the diagnostic analysis based on the available *in situ* observations and/or reanalysis datasets, and the other is the meteorological and climatological effects of spatiotemporal variability in soil moisture using numerical models. The soil moisture is usually measured by agrometeorological experimental stations. These data are mainly measured for the agriculture, which are not adequate to evaluate the interactions between the land and the atmosphere. Usually, the location of those stations did not

*Corresponding author (email: MaZG@tea.ac.cn)

take into account the impact of the diverse soil properties on soil moisture. Additionally, the spatial distribution of the stations is sparse, and the observed depth is limited. As a result, it is restricted to investigate the long-term variations in the soil moisture and its regional impact of climate change using these soil moisture datasets. Consequently, in recent years, several reanalyses of soil moisture datasets were produced by inversion and assimilation models based on satellite, radar, and other monitoring data. The reanalyses such as NCEP/NCAR, NCEP/DOE [3] and ERA40 [4] are used extensively now. Despite these restrictions, the diagnostic analysis of observations has achieved great progress. For example, Vinnikov et al. [5] reported the resolutions of soil moisture variability at different spatiotemporal levels. Li et al. [6] collected the *in situ* observations of soil moisture in China, which was frequently used for model validations and climate change studies. In China, Ma et al. [7] analyzed the spatial and temporal variations of the soil moisture and their relationship with the climate changes. Zuo [8] analyzed the relationship between variability of soil moisture and monsoon climate in East Asia and found that summer monsoon rainfall is very sensitive to spring soil moisture states. Zhang [9] investigated the spatial patterns of the soil moisture in China using several different datasets.

The *in situ* observations of soil moisture began late (in China generally began in 1980s), and spatial distribution of the stations is sparse, particularly, in the central and western China, where the terrain is complex and soil types are diverse. Some observations suggested that the variability in soil moisture is greater than the resolution of the station network. Therefore, instead of using limited observations, the numerical models play a more and more important role in the research on the variability of soil moisture and hydrological processes. Now, the soil hydrological processes of different complexity have been introduced into various hydrological components used in land surface models, ecosystem models, crop models, and so on. Generally, hydrological models [10–16] simulate runoff in catchment by formulating the processes of water cycle, whereas land surface models describe the interaction processes of land-atmosphere in the way of formulating the various processes of geophysics and geobiochemistry. Currently, the main land surface models include BATS (Biosphere Atmosphere Transfer Scheme) [17], SiB (Simple Biosphere Model) [18], SiB2 [19, 20], LSM (Land Surface Model) [21], AVIM (Atmosphere-Vegetation Interaction Model) [22], VIC (variable infiltration capacities) [23], CLM (Community Land Model) [24], etc. Soil water component was introduced into all these land surface models, among them, CLM incorporated a simplified TOPMODEL and a groundwater model, so it is comparatively comprehensive, and also it is successfully coupled to several climate system models.

Land surface model as an alternative approach to the research on the mechanism of climate change is widely adopted [25]. For example, Manabe [26] introduced a land surface hydrological model into GCM using a simplified "bucket" model to describe the land surface hydrological processes. Yeh et al. [27] showed the impact of variability of soil moisture on hydrological processes and climatic conditions through numerical experiments. Wang [28] presented the response time for climate change to variation in soil moisture by numerical experiments. Dai [29] contributed to the developments of IAP94, CLM and coupling CLM to GCM. Xie et al. [30] made progresses in parameterization of land surface hydrological processes on large spatial scale and the computational methods of groundwater level. Thus, these studies demonstrated that the development and application of numerical models provide an efficient tool to the research on the interaction between land surface progresses and climate change. Although numerical models have been greatly improved in many aspects, some physical and biochemical processes remain too simplified or unreasonably formulated. For instance, the simplified hydrological models are introduced into the land surface models in order to represent soil hydrological process, the runoff generation and confluence, but these models are too simplified to account for the impact of complex topography on the variability of soil moisture. Thus, it is a very difficult task to describe accurately the variability of soil moisture and its interaction with climate change by land surface models on the regional scale. Fortunately, the distributed hydrological models can consider the effects of topography, soil types, land use types, soil properties, and vegetation properties on soil hydrological processes with the help of high resolution DEM data. Thus, as SWAT, it can also account for the effect of some human activities on soil hydrological processes. Although the hydrological models are generally used to simulate runoff generation and confluence, they are also helpful to our investigations of soil hydrological processes in view of their advantages over land surface models in hydrological processes.

The objective of this study is to simulate the soil moisture using the distributed hydrological model SWAT. The input data used to drive the model include the *in situ* observations of atmosphere, the data on DEM, land use types, soil types, soil properties, and vegetation properties over the region of Shaanxi Province. The simulated soil moisture contains the impact of topography, soil property, land use type, and so forth on the variability of soil moisture.

## 1 SWAT model description

In this study, soil moisture is simulated by SWAT model on ARCGIS platform, namely ARCSWAT2005 [31]. SWAT is developed by Arnold et al. [32–34] for USDA-ARS (United States Department of Agriculture-Agricultural Research Service) to investigate and predict the efficiency of management measures such as irrigation, fertilization and oth-

erwise, in the complex watershed where the soil properties, land use types, and management measures change continually over a long period. SWAT is a model of comprehensive physical mechanism. It can construct model in the zone with scarce *in situ* observations, and compute efficiently at a daily time step meeting the demand of the simulation of the long-term variability of soil moisture.

SWAT was developed from SWRRB (Simulator for Water Resources in Rural Basins) [35], and some components were adapted from the models of CREAMS (Chemicals, Runoff, and Erosion from Agricultural Management Systems) [36], GLEAMS (Groundwater Loading Effects on Agricultural Management Systems) [37], EPIC (Erosion-Productivity Impact Calculator) [38]. The Penman-Monteith evapotranspiration equation and the components of snowmelt, paddy field, and marsh were introduced into SWAT successfully, and the weather generator was improved to enable the data on radiation, relative humidity, and weed speed to be read into SWAT or be generated by itself over the region where *in situ* observations are unavailable.

The following depiction is on the soil water cycle in SWAT. Precipitation is divided into two sections, the part intercepted by canopy and the part fell directly onto ground surface. The precipitation arrived at land surface is composed of soil water and surface runoff flowing into channel, and then the soil water is stored in soil or evaporates into the atmosphere or flows into surface water system through underground path. The equation formulating water cycle process is

$$SW_t = SW_0 + \sum_{i=1}^{t}(R_{\text{day}} - Q_{\text{surf}} - E_{\text{a}} - W_{\text{seep}} - Q_{\text{gw}}), \quad (1)$$

where $SW_t$ is the amount of soil moisture (mm), $SW_0$ is the initial amount of soil moisture (mm), $R_{\text{day}}$ is daily total precipitation (mm), $Q_{\text{surf}}$ is surface runoff (mm), $E_{\text{a}}$ is total evaporation (mm), $W_{\text{seep}}$ is the amount of water flowing into seepage layer (mm), and $Q_{\text{gw}}$ is the amount of water flowing into groundwater (mm).

### 1.1 Canopy interception

Canopy interception is calculated separately as a variable if surface runoff is computed by Green-Ampt method, whereas it is contained in surface runoff if surface runoff is computed by runoff curve number method. Both the maximum water storage within canopy and LAI (leaf area index) are necessary for the solution of canopy interception. Furthermore, it is assumed that the canopy interception evaporates firstly as evaporation is determined. The following is Green-Ampt equation developed by Mein and Larson in 1973.

$$f_{\text{inf},t} = K_e \cdot \left(1 + \frac{\psi_{\text{wf}} \cdot \Delta\theta_v}{F_{\text{inf},t}}\right), \quad (2)$$

$$F_{\text{inf},t} = F_{\text{inf},t-1} + R_{\Delta t}, \quad (3)$$

where $f_{\text{inf},t}$ is the infiltration rate (mm/h) at time $t$, $K_e$ is the effective hydraulic conductivity (mm /hr), $\psi_{\text{wf}}$ is the wetting front matric potential (mm), $\Delta\theta_v$ is the change in moisture content across the wetting front (mm/mm), $F_{\text{inf},t}$ is the cumulative infiltration (mm) at time $t$, and $R_{\Delta t}$ is the precipitation during the time step (mm). In order to avoid numerical errors over long time steps, and $F_{\text{inf},t}$ is replaced by $\mathrm{d}f_{\text{inf}}/\mathrm{d}t$ in eq. (2), then

$$F_{\text{inf},t} = F_{\text{inf},t-1} + K_e \cdot \Delta t + \psi_{wf} \cdot \Delta\theta_v \cdot \ln\left[\frac{F_{\text{inf},t} + \psi_{wf} \cdot \Delta\theta_v}{F_{\text{inf},t-1} + \psi_{wf} \cdot \Delta\theta_v}\right], \quad (4)$$

$$K_e = \frac{56.82 \cdot K_{\text{sat}}^{0.286}}{1 + 0.051 \cdot \exp(0.062 \cdot CN)} - 2, \quad (5)$$

$$\begin{aligned}\psi_{wf} = 10 \cdot \exp[&6.5309 - 7.32561 \cdot \phi_{\text{soil}} + 0.001583 \cdot m_c{}^2 \\ &+3.809479 \cdot \phi_{\text{soil}}{}^2 + 0.000344 \cdot m_s \cdot m_c \\ &-0.049837 \cdot m_s \cdot \phi_{\text{soil}} + 0.001608 \cdot m_s{}^2 \cdot \phi_{\text{soil}}{}^2 \\ &+0.001602 \cdot m_c{}^2 \cdot \phi_{\text{soil}}{}^2 - 0.0000136 \cdot m_s{}^2 \cdot m_c \\ &-0.003479 \cdot m_c{}^2 \cdot \phi_{\text{soil}} - 0.000799 \cdot m_s{}^2 \cdot \phi_{\text{soil}}],\end{aligned} \quad (6)$$

where $K_{\text{sat}}$ is the saturated hydraulic conductivity (mm/h), $CN$ is the curve number, $\phi_{\text{soil}}$ is the porosity of the soil (mm/mm), $m_c$ is the percentage clay content, and $m_{\text{s}}$ is the percentage sand content.

### 1.2 Surface runoff

SWAT simulates surface runoff and peak runoff rate for each hydrological response unit (HRU) using daily or sub-daily precipitation. Surface runoff is calculated by the modification of the SCS curve number method, in which the curve number changes nonlinearly as soil water is below wilting point or equal to saturation. Also surface runoff can be calculated by the Green-Ampt method, if daily or sub-daily precipitation is available.

### 1.3 Transmission losses

Transmission losses take place in ephemeral and intermittent streams, and SWAT calculates it by experiential methods. The losses are associated with the function of channel width, length, and flow duration, and runoff and peak rate are adjusted as transmission occurs in tributary channel.

### 1.4 Evapotranspiration

Evapotranspiration comprises principally evaporation from soil and canopy, transpiration and evaporation from water surface. Evaporation from soil and transpiration are simu-

lated separately. The potential evaporation from soil is estimated from potential transpiration by LAI. The actual evaporation from soil is calculated by the exponential function of soil depth and soil moisture content. Transpiration from canopy is calculated by the linear function of potential transpiration and LAI, and the function can be formulated by Hargreaves, Priestley-Tayl, and Penman-Monteith. Among three, Penman-Monteith is adopted extensively.

### 1.5 Percolation

The calculation of percolation needs to consider two main variables, the initial percolation rate and the maximum percolation rate. Percolation cannot be calculated directly since a daily time step is adopted in runoff curve number method in SWAT. Nevertheless, it can be determined indirectly by the difference of precipitation minus surface runoff. If the observed precipitation at high temporal resolution is available, percolation can be calculated directly by Green-Ampt method.

### 1.6 Redistribution

Redistribution is the spread of water in soil after the percolation of surface water generated from precipitation or irrigation, and it takes place for the reason of the irregular distribution of soil water. The redistribution component in SWAT uses a storage routing technique to forecast soil water flux through each soil layer. Percolation occurs when the amount of soil water stored in a soil layer exceeds the field capacity, but the underlying layer is not saturated. Percolation rate is determined by the saturated conductivity of the soil layer, and it is also influenced by soil temperature. Therefore, redistribution is suspended, when the temperature in the soil layer is below 0°C.

### 1.7 Interflow

Interflow in each soil layer is calculated by the kinematic storage model synchronizing with the calculation of redistribution. Moreover, the kinematic storage model considers the influence of the changes of conductivity, slope, and soil moisture content on interflow.

### 1.8 Underground water

In SWAT, underground water is composed of water stored in shallow aquifer and in deep aquifer. Water in shallow aquifer enters streams within the watershed finally, or it is absorbed directly by plant roots partly or transmitted to the unsaturated soil layers. The deep aquifer water flows into streams beyond the watershed. The water balance for shallow aquifer is

$$aq_{\mathrm{sh},i}=aq_{\mathrm{sh},i-1}+w_{\mathrm{rchrg,sh}}-Q_{\mathrm{gw}}-w_{\mathrm{revap}}-w_{\mathrm{pump,sh}}. \quad (7)$$

where $aq_{\mathrm{sh},i}$ and $aq_{\mathrm{sh},i-1}$ are the amount of water in the shallow aquifer on day $i$ and $i$–1 respectively(mm), $w_{\mathrm{rchrg,sh}}$ is the amount of recharge entering shallow aquifer (mm), $Q_{\mathrm{gw}}$ is groundwater flowing into main channel (mm), $w_{\mathrm{revap}}$ is the amount of water moving into the soil zone (mm), and $w_{\mathrm{pump,sh}}$ is the amount of water removed from the shallow aquifer by pumping (mm). The water balance for deep aquifer is

$$aq_{\mathrm{dp},i}=aq_{\mathrm{dp},i-1}+w_{\mathrm{deep}}-w_{\mathrm{pump,dp}}, \quad (8)$$

where $aq_{\mathrm{dp},i}$ and $aq_{\mathrm{dp},i-1}$ are the amount of water stored in deep aquifer on day $i$ and $i$–1 respectively (mm), $w_{\mathrm{deep}}$ is the amount of water percolating from shallow aquifer into deep aquifer (mm), $w_{\mathrm{pump,dp}}$ is the amount of water removed from the deep aquifer by pumping (mm).

Other detailed depictions of the physical processes adopted in SWAT can be found in the SWAT theoretical documentation [39].

## 2 Forcing data

The data on DEM, soil types, land use types, and stream network used to drive the SWAT is derived from national dataset on the scale of 1 to 400 million. In our study region, there are 16 soil types such as brown earths, cinnamon soils, etc, and 9 land use types such as paddy field, woodland, grassland, and so on. Other input data such as the soil properties, vegetation types, and atmospheric observations needed to drive the model are described below.

The soil particle size and percentage of different soil types from the *National Soil Investigation* are interpolated with weighted fitting method. Soil bulk density, field capacity, wilting point, and saturated hydraulic conductivity are simulated by SPAW model. Albedo is estimated following the approaches in earlier studies [40–42] and the empirical relationship between albedo and the soil moisture. The factor of soil erosion is calculated with the equation developed by Wischmeier et al. [43] in 1971:

$$K_{\mathrm{USLE}}=\frac{0.00021\cdot M^{1.14}\cdot(12-OM)+3.25\cdot(C_{\mathrm{soilstr}}-2)+2.5\cdot(C_{\mathrm{perm}}-3)}{100}, \quad (9)$$

where $M$ is the percentage relating to soil particle size.

$$M=(m_{\mathrm{silt}}+m_{\mathrm{vfs}})\cdot(100-m_c), \quad (10)$$

$m_{\mathrm{silt}}$ is the percentage of the soil particle size between 0.002 and 0.05 mm, $m_{\mathrm{vfs}}$ is the percentage of the soil particle size between 0.05 and 0.1 mm, $m_c$ is the percentage of the soil particle size less than 0.002 mm, and $OM$ is the percentage of soil organic matter; the formula of the percentage with observed carbon is

$$OM = 1.72 \cdot orgC, \quad (11)$$

$C_{\text{soilstr}}$ is the code of soil types; $C_{\text{perm}}$ is the grade of soil infiltration [44].

The data on local vegetation properties is the same as that in SWAT. The meteorological data used include daily maximum and minimum temperature, solar radiation, wind speed, relative humidity, and precipitation [44] during 1951–2004. For stations without solar radiation observation, or with missing observations, the solar radiation is estimated using observed cloud cover at the same station. The relative humidity is estimated using observed water vapor pressure data.

## 3 Simulation, validation, and comparative analysis

### 3.1 Study area

In our study, we investigate the variability of soil moisture by simulating soil moisture content with SWAT in Shaanxi Province, which spans three climatic zones such as humid climate, subhumid climate, and semiarid climate in terms of precipitation. Shaanxi Province is composed, from north to south, of the north Shaanxi plateau, the central Shaanxi plain, and the Qinling-Daba mountainous region. The terrain is a variation of the loess plateau, alluvial plains, mountainous regions, basins and so forth. The complex terrain and climate are very helpful in validating the simulation ability of the model SWAT. Although, in hydrological models, study area is determined by watershed generally, here the area of interest is more like an administrative area. The inaccuracy induced by the selection method for the area of interest has a negligible influence on the simulation of soil moisture, if the inlets and outlets of streams are located reasonably, and small tributaries are contained entirely before the subbasin delineation. Furthermore, the focus of this study is on the variability of soil moisture but not the flow, and also it is more convenient to evaluate the effects of human activities to select an approximate administrative area as the domain of study.

### 3.2 Simulation and validation

In this study, the HRUs and subbasins are delineated by SWAT in Shaanxi Province, based on the national data on DEM, soil types, land use types, and stream network. The delineation accuracy of stream network and subbasins is relevant to the size of area used to define the origin of a stream, which is specified manually. The smaller the area is selected, the more detailed stream network and subbasins are generated. However, the precision of the data on DEM, soil types, and land use types as well as computational efficiency should be taken into account. A single subbasin comprises several HRUs determined by the properties of soil and land use types, or it is monopolized by one HRU specified by the dominant property. In this study, 412 subbasins (the same number as HRUs) were generated for our target region, and the total amount of soil water in the entire soil layer, soil moisture content in each soil layer and soil evaporation are output separately during 1951–2004.

The *in situ* observations of soil moisture at 12 agrometeorological stations are used to evaluate the soil moisture simulations. Locations and measurements of the 12 stations can be found at Figure 1 and Table 1.

The soil moisture in the above 12 stations is usually measured three times a month, on the 8th, 18th, and 28th days. Thus, we compare the observed with the modeled soil moisture at the corresponding days to evaluate the model simulations. Figure 2 shows the fluctuations of 418 observed soil moisture contents and corresponding modeled contents in 1–10 cm soil layers from 1987 to 2002 for Suide station. Here the observed soil moisture content is estimated by the following equation:

$$mm\text{H}_2\text{O} = dz_{\text{soil}} \cdot \rho_{\text{soil}} \cdot w \cdot 10\,, \quad (12)$$

where $dz_{\text{soil}}$ is the depth of soil layer (mm), $\rho_{\text{soil}}$ is the density of the measured soil (g/cm$^3$), and $w$ is the observed percentage of the weight of soil water to the weight of dry soil.

To evaluate the model simulations, the correlation coef-

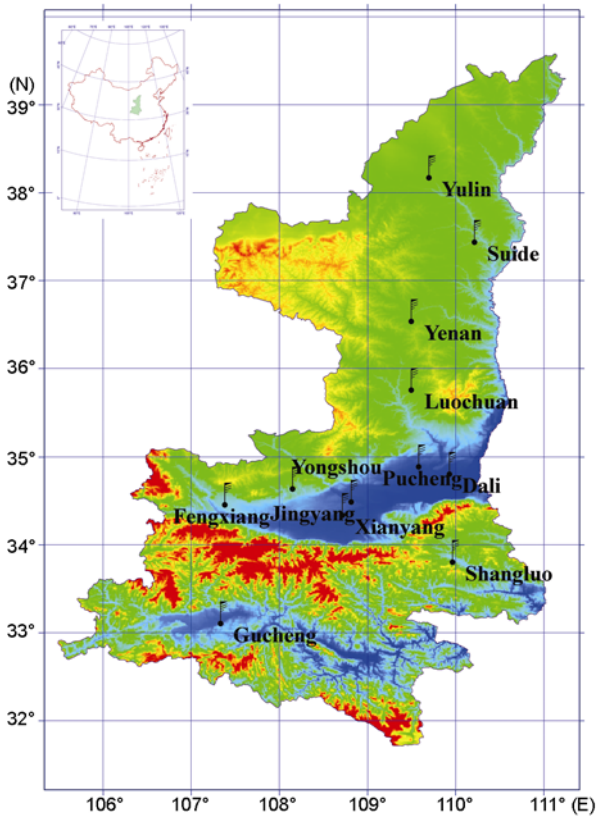


**Figure 1** Locations of stations over the study area.

ficients as well as the root mean square error between the modeled and observed soil moisture content are computed.

$$RMSE = \sqrt{\frac{\sum_{i=1}^{n}(\mathrm{SWAT}_i - \mathrm{Obs}_i)^2}{n}}, \quad (13)$$

where *RMSE* is the root mean square error, $\mathrm{SWAT}_i$ is the modeled soil moisture content, $\mathrm{Obs}_i$ is the observed soil moisture content, and $n$ is the number of samples.

Table 2 suggested that the modeled soil moisture contents on all soil layers are significantly correlated to the observations, indicating that the model can reasonably simulate the variations of the observed soil moisture contents. However, the RMSE between the modeled and observed soil moisture contents is large, possibly because the definitions of observed and modeled soil moisture contents are different. The observation is estimated by percentage of weight, whereas the modeled is defined by the millimeter depth of the total water stored in a soil layer. Another rea-

**Table 1** Stations and observation periods

| Station | Latitude (°N) | Longitude (°E) | Altitude (m) | Begin year | End year | Missing year |
|---|---|---|---|---|---|---|
| Yulin | 38.233 | 109.7 | 1057.5 | 1987 | 2002 | |
| Suide | 37.5 | 110.217 | 929.7 | 1987 | 2002 | |
| Yenan | 36.6 | 109.5 | 1000.0 | 1982 | 2002 | |
| Luochuan | 35.817 | 109.5 | 1159.8 | 1990 | 2002 | 1992 |
| Pucheng | 34.95 | 109.583 | 499.9 | 2001 | 2002 | |
| Fengxiang | 34.517 | 107.383 | 781.8 | 2001 | 2002 | |
| Yongshou | 34.7 | 108.15 | 994.6 | 1990 | 2002 | |
| Jingyang | 34.55 | 108.817 | 427.4 | 1981 | 1989 | |
| Dali | 34.867 | 109.933 | 368.4 | 1990 | 2002 | |
| Xianyang | 34.4 | 108.717 | 472.8 | 1990 | 2002 | |
| Chenggu | 33.167 | 107.333 | 487.0 | 2001 | 2002 | |
| Shangluo | 33.867 | 109.967 | 743.8 | 2001 | 2002 | |

**Table 2** Values for *R* and *RMSE* between observed and modeled soil moisture contents[a)]

| | 0–10 cm | 10–20 cm | 20–30 cm | 30–50 cm | 50–80 cm | 80–100 cm |
|---|---|---|---|---|---|---|
| *R* | 0.740** | 0.624** | 0.583** | 0.516** | 0.528** | 0.383** |
| *RMSE* | 7.030 | 7.452 | 5.671 | 13.702 | 24.872 | 18.874 |

a) *R* is correlation coefficient; *RMSE* is root mean square error, ** indicates the significant correlation at 0.01 level, the same below.

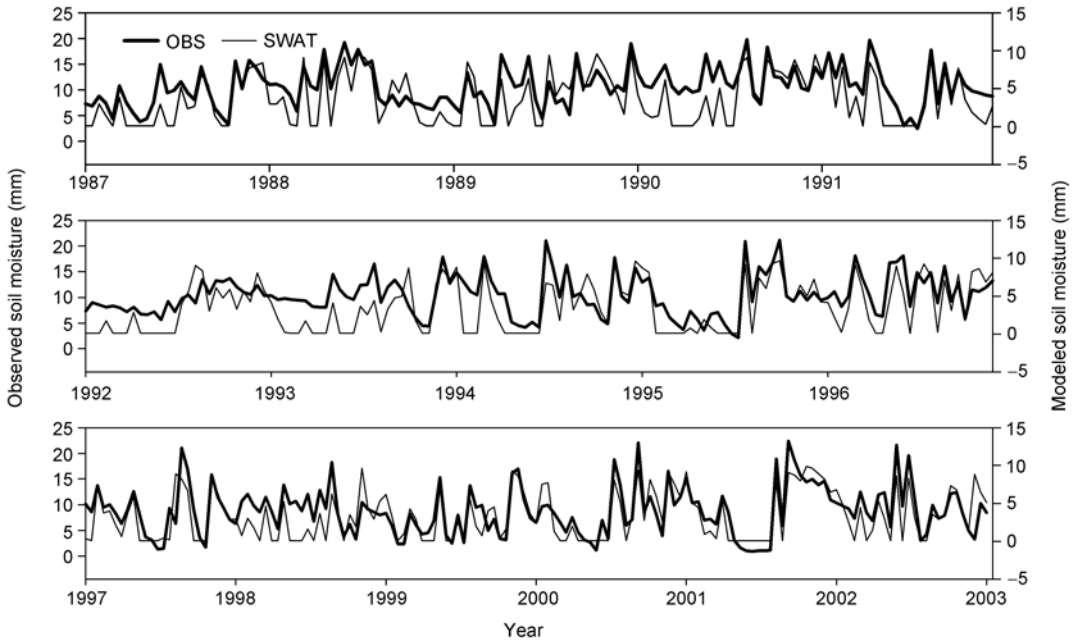


**Figure 2** Comparison of the observed and modeled soil moisture contents in 0–10 cm layer.

son for the difference is that the modeled soil moisture is the averaged soil moisture over a HRU, while the observation is measured at a given site. Therefore, in the following, we merely compare the variations in the modeled and observed soil moisture contents, while the mean values of the soil moisture is not considered.

Figures 3 and 4 compare the observed and modeled soil moisture contents for two layers (0–10 and 0–100 cm) during 1987–2002 for Suide station. To facilitate a better comparison, both the observed and modeled soil moisture contents are normalized for the period of 1987–2002. The time series of normalized soil moisture indicate that the variations of the modeled soil moisture agree well with the observations.

The correlation coefficients between observed and modeled soil moisture contents on various layers for all the 12 stations are summarized in Table 3. Generally, the variations of modeled soil moisture contents correlate significantly with the observations on various soil layers at most stations.

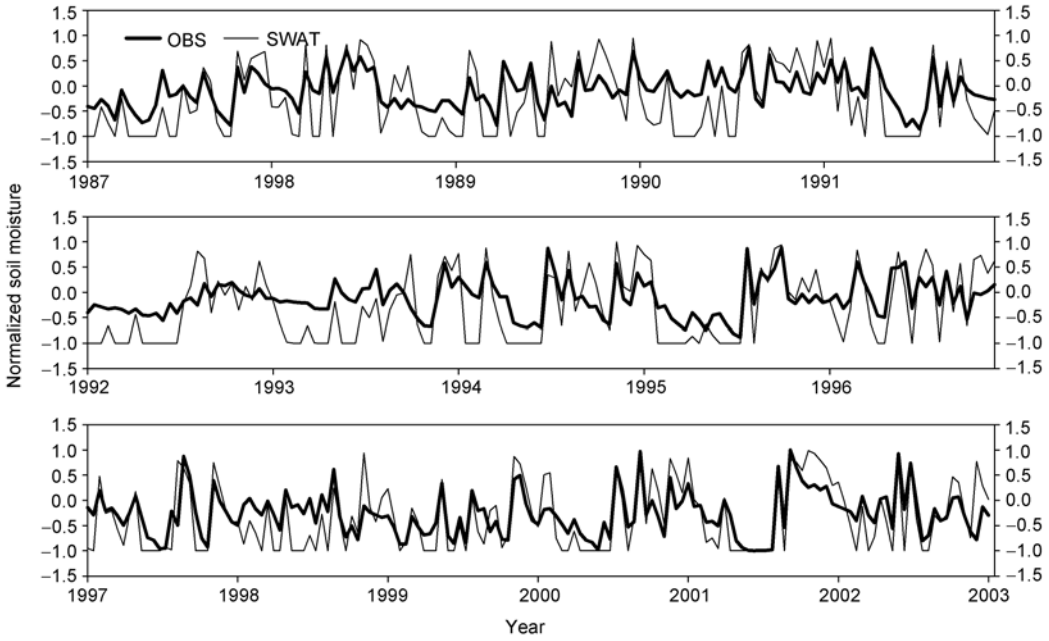


**Figure 3** Comparison of observed and modeled soil moisture contents normalized in 0–10 cm layer.

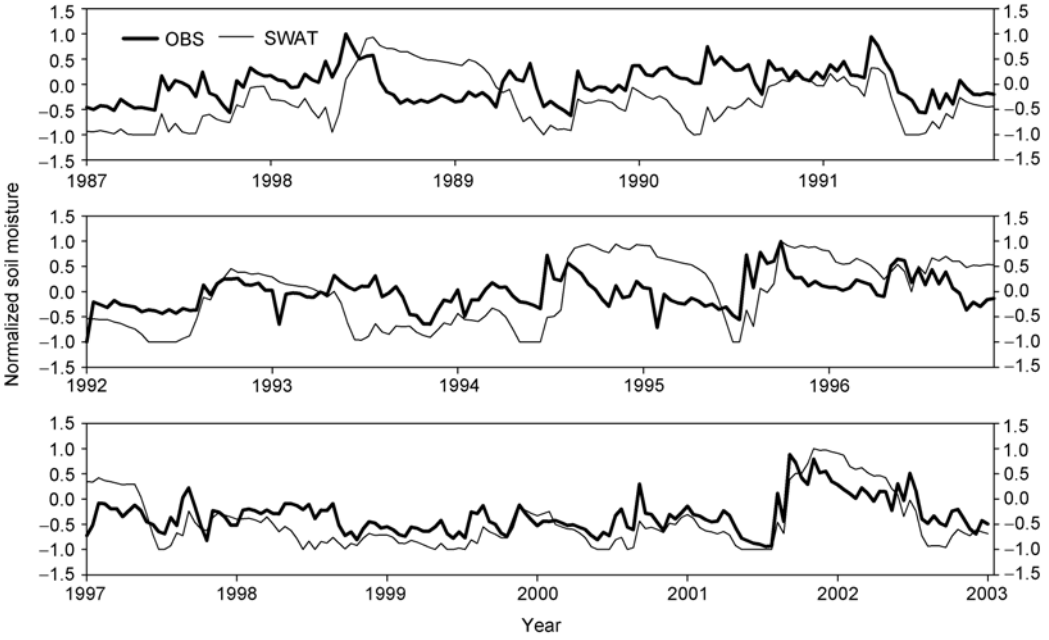


**Figure 4** Comparison of observed and modeled soil moisture contents normalized in 0–100 cm layer.

The monthly means of observed and modeled soil moisture contents are also compared to evaluate the reliability of the model. Figure 5 compares the observed and modeled monthly averaged soil moisture at Fengxiang station during 2001–2002. The fluctuations of the modeled and observed soil moisture time series are generally consistent with each other.

The correlation coefficients between the observed and modeled monthly soil moisture contents are shown in Table 4. The correlation suggests that the variations of modeled and observed soil moisture agreed reasonably well with each other at monthly time scale.

The model performance is further evaluated by comparing the observed and model annual averaged soil moisture

**Table 3** Correlation coefficients between observed and modeled soil moisture contents[a)]

| Station | 0–10 cm | 10–20 cm | 20–30 cm | 30–50 cm | 50–80 cm | 80–100 cm | 0–100 cm |
|---|---|---|---|---|---|---|---|
| Yulin | 0.534** | 0.366** | 0.229** | 0.082 | 0.005 | 0.119* | 0.164** |
| Suide | 0.740** | 0.624** | 0.583** | 0.516** | 0.528** | 0.383** | 0.546** |
| Yenan | 0.625** | 0.483** | 0.367** | 0.388** | 0.485** | 0.482** | 0.604** |
| Luochuan | 0.518** | 0.475** | 0.377** | 0.437** | 0.420** | 0.455** | 0.618** |
| Pucheng | 0.357** | 0.423** | 0.308** | 0.398** | 0.406** | 0.515** | 0.383** |
| Fengxiang | 0.511** | 0.646** | 0.699** | 0.708** | 0.661** | 0.567** | 0.791** |
| Yongshou | 0.150** | 0.108* | 0.088 | 0.059 | 0.017 | –0.041 | 0.027 |
| Jingyang | 0.520** | 0.471** | 0.454** | 0.446** | 0.579** | 0.570** | 0.623** |
| Dali | 0.308** | 0.291** | 0.237** | 0.134** | NaN | NaN | 0.382** |
| Xianyang | 0.670** | 0.449** | 0.410** | 0.380** | 0.538** | 0.504** | 0.648** |
| Chenggu | 0.730** | 0.638** | 0.519** | 0.526** | NaN | NaN | 0.444** |
| Shangluo | 0.655** | 0.454** | 0.492** | 0.316** | NaN | NaN | 0.250* |

a) NaN marks no value because of the missing observed, * indicates the significant correlation at 0.05 level, the same below.

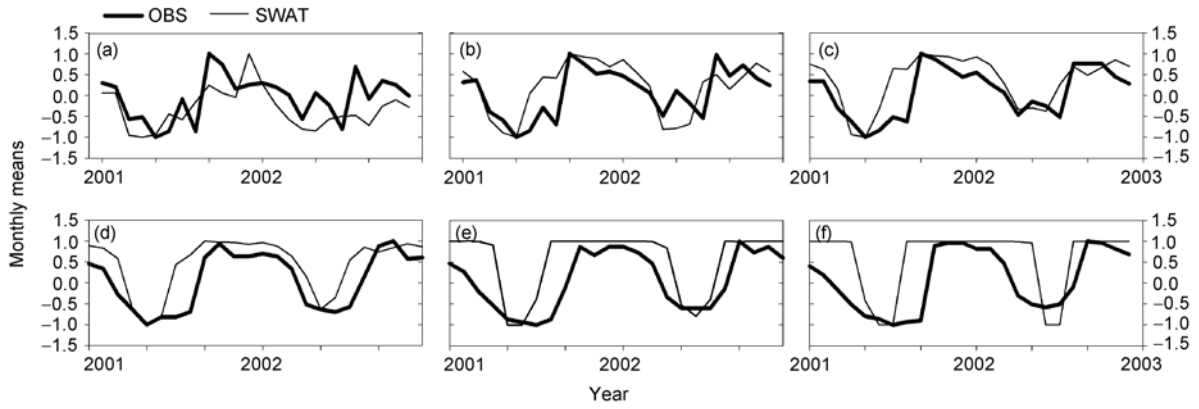


**Figure 5** Comparisons of the monthly means of soil moisture observed and simulated. (a)–(f) indicate 0–10, 10–20, 20–30, 30–50, 50–80, 80–100 cm, 6 soil layers respectively.

**Table 4** Correlation coefficients between monthly means of observed and simulated soil moisture contents

| Station | 0–10 cm | 10–20 cm | 20–30 cm | 30–50 cm | 50–80 cm | 80–100 cm | 0–100 cm |
|---|---|---|---|---|---|---|---|
| Yulin | 0.499** | 0.343** | 0.241* | 0.049 | –0.011 | 0.072 | 0.118 |
| Suide | 0.664** | 0.550** | 0.521** | 0.451** | 0.523** | 0.394** | 0.528** |
| Yenan | 0.586** | 0.439** | 0.338** | 0.401** | 0.514** | 0.509** | 0.621** |
| Luochuan | 0.478** | 0.417** | 0.338** | 0.448** | 0.449** | 0.492** | 0.598** |
| Pucheng | 0.179 | 0.370 | 0.170 | 0.441* | 0.409* | 0.513** | 0.369 |
| Fengxiang | 0.575** | 0.687** | 0.777** | 0.802** | 0.715** | 0.580** | 0.823** |
| Yongshou | 0.211* | 0.147 | 0.114 | 0.094 | 0.076 | –0.068 | 0.062 |
| Jingyang | 0.483** | 0.424** | 0.480** | 0.447** | 0.597** | 0.583** | 0.618** |
| Dali | 0.192 | 0.242* | 0.223* | 0.144 | NaN | NaN | 0.396** |
| Xianyang | 0.586** | 0.393** | 0.413** | 0.397** | 0.566** | 0.549** | 0.658** |
| Chenggu | 0.829** | 0.688** | 0.534** | 0.582** | NaN | NaN | 0.497** |
| Shangluo | 0.698** | 0.459* | 0.503** | 0.359 | NaN | NaN | 0.218 |

contents at the stations with longer than 7 years observations. The comparisons between the observed and modeled annual soil moisture contents at Yongshou during 1987–2002 are shown in Figure 6. The time series suggest that the modeled variations capture the feathers of the interannual variations of observations in general.

The correlation coefficients between the observed and modeled annual means for soil moisture contents are listed in Table 5. Compared to the correlation between monthly means of modeled and observed soil moisture, the correlation between annual means is decreased. Nevertheless, most of the correlation coefficients are positive, even significant at $\alpha$=0.01 (or $\alpha$=0.05) level.

Table 3 shows that the correlation between the observed and modeled soil moisture contents at the 12 stations are usually significant at the 95% or higher confidence level, so does the correlation between the observed and modeled monthly and annual averaged soil moisture (Tables 4 and 5). For example, the correlations between observed and modeled soil moisture contents are statistically significant at $\alpha$=0.01 level on 79% of the stations and soil layers. This number increases to 83% when the correlations are measured at $\alpha$=0.05 level. When the soil moisture are monthly averaged, the correlations between modeled and observed soil moisture contents (SMC) are significant at $\alpha$=0.01 ($\alpha$=0.05) level on 63% (71%) of the stations and soil layers. The correlation coefficients between annual means are not statistically significant mostly, because the sample numbers at some stations are too small, for example, 20 years only at 3 stations, 12 or 13 years at 4 stations, 7 years at 1 station, and only 2 years at other 4 stations. Under such conditions, the correlation analysis cannot completely exhibit the actual relationship between observed and simulated soil moisture. In summary, correlation analyses suggested that the model can reasonably simulate the observed soil moisture variations. The model simulation is better on shallow soil layers than on deep soil layers. Additionally, the model simulations are better on the daily time scale than those on the monthly and annual time scales. The model, however, underestimates the mean soil moisture contents, possibly related to unit conversion, varying soil density, and imperfect model components.

### 3.3 Comparison between the SWAT simulations and the soil moistures in the Reanalyses

To evaluate the model performance, we also compare the SWAT model simulations with the soil moistures of NCEP/NCAR and ERA40 reanalyses. The observations used for the evaluations are the averages of the six stations with long and complete measurements. For SWAT model, the six HRUs where the six stations are located were chosen, while for the reanalysis, three grid points from NCEP/NCAR and two grid points from EAR40 nearby the six sta-

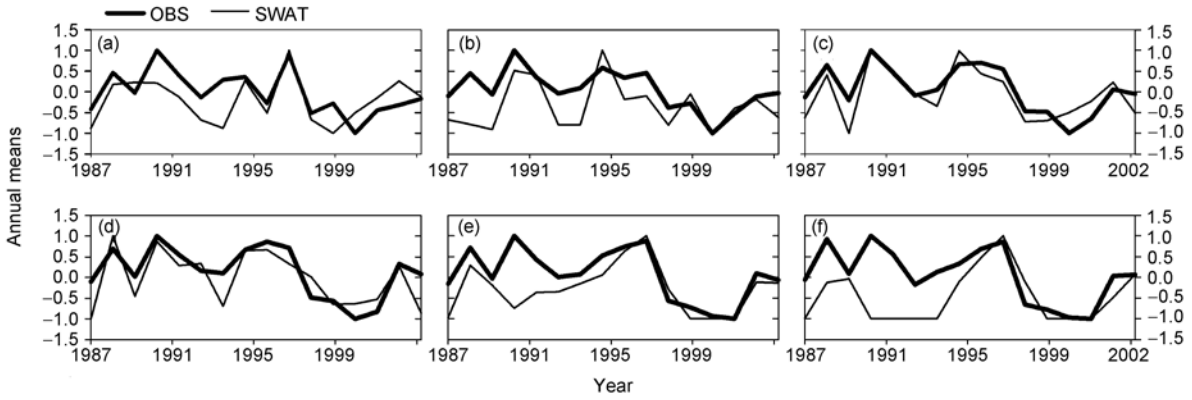


**Figure 6** Comparisons between the annual soil moisture observed and modeled. (a)–(f) indicate the fluctuations of annual soil moisture contents in 0–10, 10–20, 20–30, 30–50, 50–80 and 80–100 cm soil layers respectively.

**Table 5** Correlation coefficients between annual means of observed and simulated soil moisture contents in various soil layers

| Station | 0–10 cm | 10–20 cm | 20–30 cm | 30–50 cm | 50–80 cm | 80–100 cm | 0–100 cm |
|---|---|---|---|---|---|---|---|
| Yulin | 0.600** | 0.316 | 0.144 | 0.237 | 0.136 | 0.316 | 0.323 |
| Suide | 0.601** | 0.637** | 0.822** | 0.754** | 0.698** | 0.453 | 0.701** |
| Yenan | 0.581** | 0.611** | 0.563** | 0.581** | 0.556** | 0.511* | 0.630** |
| Luochuan | 0.283 | 0.171 | 0.081 | 0.170 | 0.152 | 0.199 | 0.234 |
| Yongshou | –0.072 | –0.092 | –0.202 | –0.116 | 0.046 | –0.043 | –0.053 |
| Jingyang | 0.758* | 0.614 | 0.553 | 0.413 | 0.814** | 0.772* | 0.796* |
| Dali | 0.617* | 0.498 | 0.613* | 0.193 | NaN | NaN | 0.434 |
| Xianyang | 0.568* | 0.684** | 0.463 | 0.171 | 0.353 | 0.233 | 0.536* |

tions were used. Figure 7 shows the comparisons of the observed, modeled and the reanalysis SMC on monthly and annual average in the Shaanxi Province. For a better comparison, all the SMC shown on the figure were normalized.

The correlation between the observed soil moisture contents, the NCEP/NCAR and ERA40 reanalyses and the simulated by SWAT are shown in Table 6.

Figure 7 and Table 6 suggest that, compared to the NCEP/NCAR and EAR40 reanalyses, the SWAT model is the best in simulating the variations of the observed SMC on daily, monthly, and annual time scale. The long-term trend coefficients in soil moisture of the observations, the modeled, the NCEP /NCAR and ERA40 reanalyses are –0.1106, –0.0591, –0.0560, and –0.0181 respectively, suggested an overall weak decreasing SMC during 1990–2002. The simulated soil moisture by SWAT agrees better with the observed than NCEP/NCAR and ERA40 reanalyses. Interannual variability of the soil moisture shows that the fluctuation of observed soil moisture is small during 1990–1993, then became larger from 1993 to 1998, and became small again from 1998 to 2002. The SWAT reproduced these changes, whereas the NCEP/NCAR and ERA40 reanalyses showed almost constant amplitudes of fluctuations, and underestimated the variability of the observations.

The above comparisons suggested that the SWAT is better than the two reanalyses in simulating the observed variations and long-term trend of soil moisture in Shaanxi Province, which assures us to investigate the variability of soil moisture and its interaction with climate change on regional or watershed scales.

## 4 Distribution pattern and long-term trend of soil moisture during 1951–2004

The SWAT was then used to simulate the soil moisture in Shaanxi Province during 1951–2004. Figure 8 shows the spatial distribution of the 54–year averaged SMC on various soil layers in Shaanxi Province. Generally, low SMC appeared between the Great Wall and the Mu Us desert, whereas high SMC is observed on the river basins, e.g., the Luohe river basin, the Jinghe river basin, the Weihe river basin, and the Hanshui rive basin. On shallow soil layers, high SMC is located over the Baiyushan and Qinling-Daba mountainous regions where many rivers originate. The SMC there is even higher than that over the central Shaanxi plain and the Hanshui valley. This spatial distribution of SMC on shallow layers is closely controlled by precipitation, terrain, and ecological environment. For example, the Qinling Mountains are the climatic and watershed boundary between the northern and southern China. The primary water sources for southern and central Shaanxi originate in the Qinling Mountains, a region with high vegetation cover, frequent orographic precipitation, and less anthropogenic influence. For deeper soil, high soil moisture contents mainly occurred in the large river basins, e.g., in the Luohe river basin, the Jinghe river basin, the Weihe river basin, and the Hanshui river basin.

Figure 9 shows the temporal variations of the soil moisture contents on different soil layers over the last 54 years. The slope coefficients of regression lines for 54-year fluctuations of soil moisture are –0.006, –0.064, –0.071, –0.176, –0.353, –0.310 in 1–10, 10–20, 20–30, 30–50, 50–80, 80–100 cm soil layers over the zone north of the Qinling Mountains respectively, and those counterparts over the

**Table 6** Correlation coefficients of NCEP/NCAR, ERA40, and SWAT with observations

| | SWAT | NCEP | ERA40 |
|---|---|---|---|
| Daily | 0.673** | 0.343** | 0.565** |
| Monthly mean | 0.648** | 0.296** | 0.512** |
| Annual mean | 0.754** | 0.434 | 0.631* |

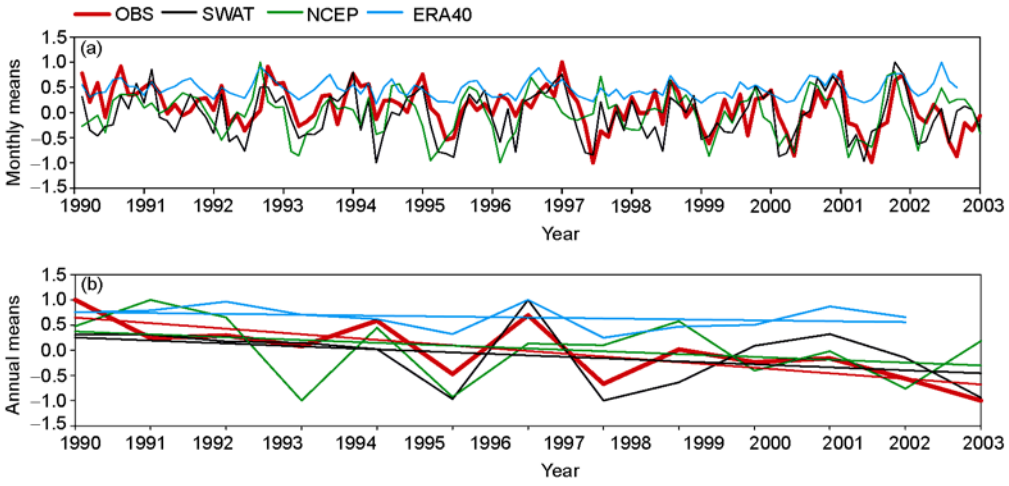


**Figure 7** Comparisons between monthly and annual means of observations, NCEP/NCAR, ERA40 reanalyses and SWAT Simulations. (a) Monthly averaged series; (b) annual averaged series and linear trends.

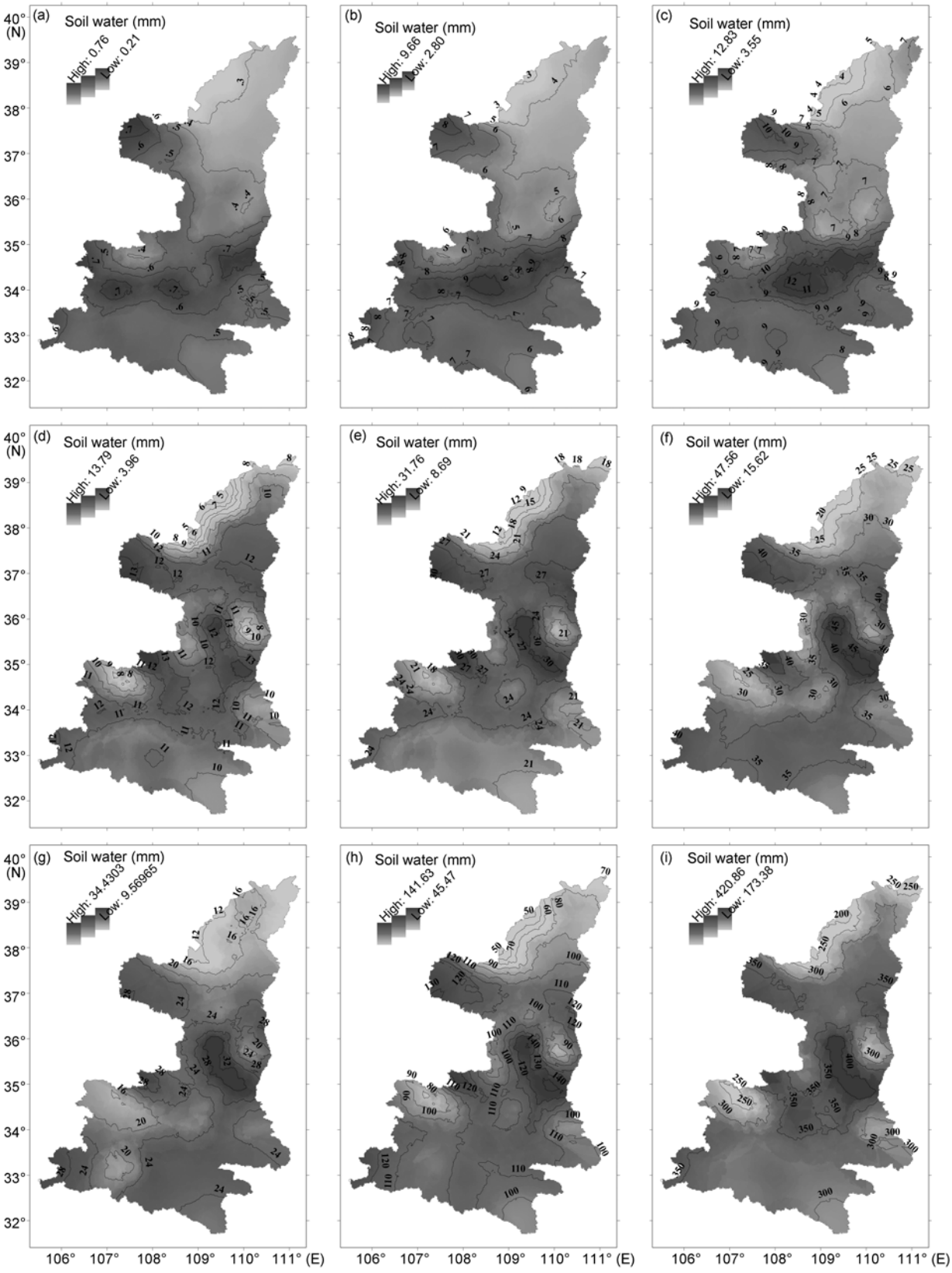


**Figure 8** The spatial distribution of 54-year mean soil moisture by SWAT in different depths. (a)–(f) indicate the distribution pattern of soil moisture in 0–1, 1–10, 10–20, 20–30, 30–50, 50–80, 80–100, 0–100, 0–2500 cm soil layers respectively.

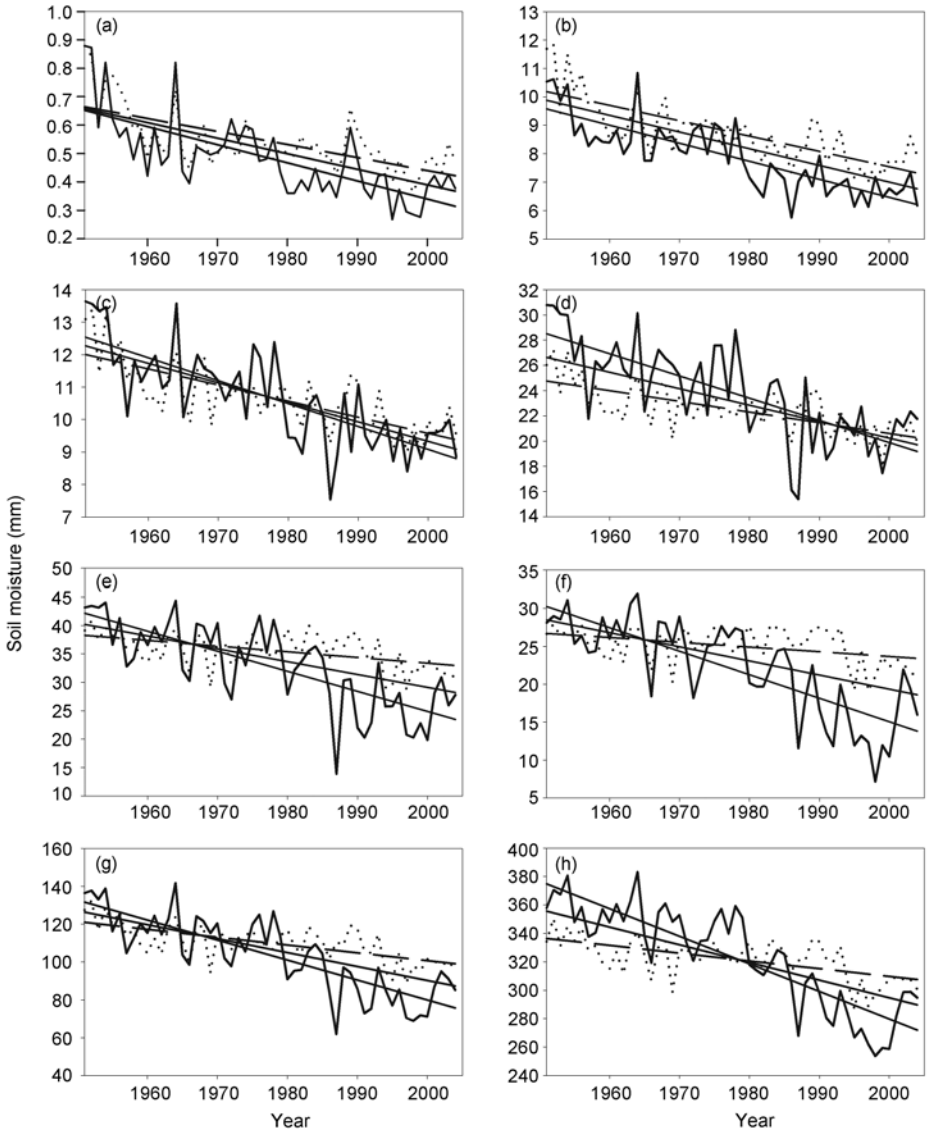


**Figure 9** The trends in the 54-year soil moisture over the regions north and south of the Qinling Mountains. (a)–(h) indicate the trend of spatial mean soil moisture in 1–10, 10–20, 20–30, 30–50, 50–80, 80–100, 0–100, 0–2500 cm soil layers.

zone south of the Qinling Mountains are –0.005, –0.054, –0.050, –0.085, –0.100, –0.062 respectively. Decreasing trends are found on all soil layers during the last 54 years, with the trend stronger in regions north of the Qinling Mountains. Moreover, the rates of decreasing trend become stronger with the soil depths. The decreasing trend in soil moisture is also consistent with the observations during 1990–2002, as shown in Figure 10. These results indicated that the soil in Shaanxi dehydrates gradually from surface to deeper soil layers. The decreasing soil moisture is likely related to decreasing precipitation and the increasing surface air temperature in the region. Figures 11 and 12, respectively, show temporal variations of the daily total precipitation and daily mean temperature averaged over regions on the north and south of the Qinling Mountains during 1951–2004. Figure 11 suggests that the precipitation is

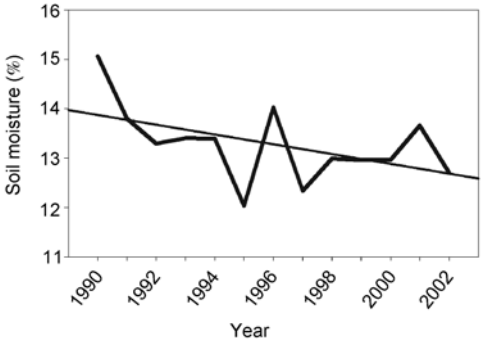


**Figure 10** The trend in the 13-year observed soil moisture.

decreasing (the slope coefficients are –0.035 and –0.024) on both the north and south of the Qinling Mountains. Intense decreases in precipitation occurred at the end of 1970s to

the beginning of 1980s, likely led to intense decreases in the SMC. Figure 12 shows that temperature warms up gradually over the past 54 years, with stronger warming north of the Qinling Mountains. The temperature warms up faster after 1980s, consistent with the decreasing precipitation and the SMC.

In order to represent the spatial distribution of variation trends in soil moisture, we calculate the trend coefficients to determine the soil moisture increases or decreases for 412 HRUs respectively over the 54-year period. The trend coefficient is the correlation coefficient between annual mean soil moisture $\{SW_{HRU,i}\}$($HRU$=1, 2, …, 412; $i$=1, 2, …, 54) and a sequence of natural numbers {1, 2, 3, …, 54}, and it is formulated as eq. (14)

$$R_{HRU} = \frac{\sum_{i=1}^{n}(sw_{HRU,i} - \overline{sw_{HRU}})(i - \bar{t})}{\sqrt{\sum_{i=1}^{n}(sw_{HRU,i} - \overline{sw_{HRU}})^2 \sum_{i=1}^{n}(i - \bar{t})^2}}, \quad (14)$$

where $R_{HRU}$ is trend coefficient for $HRU$, $\overline{sw}_{HRU}$ is the 54-year mean of observed soil moisture over a $HRU$, $\bar{t}$ is the mean of the sequence of natural numbers, $n$ is the size of the sequence, here $n$=54. In the case of $R_{HRU}$>0, it indicates that the soil moisture trends up, while $R_{HRU}$<0, it indicates that the soil moisture trends down, as $R_{HRU}$=0, it indicates soil moisture has no variation. Figure 13 shows the spatial distribution of long-term trends of the soil moisture contents on various soil layers for 412 HRUs during the past 54 years.

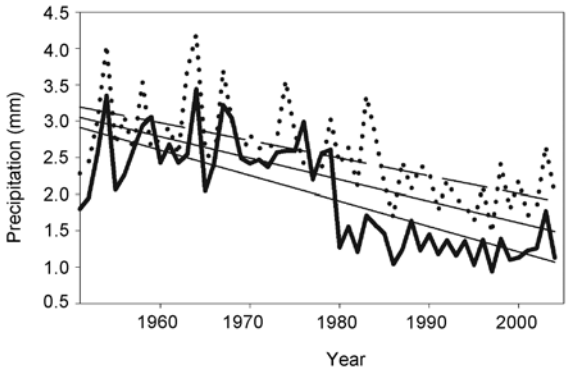


**Figure 11** The trends in the 54-year precipitation over regions north and south of the Qinling Mountains.

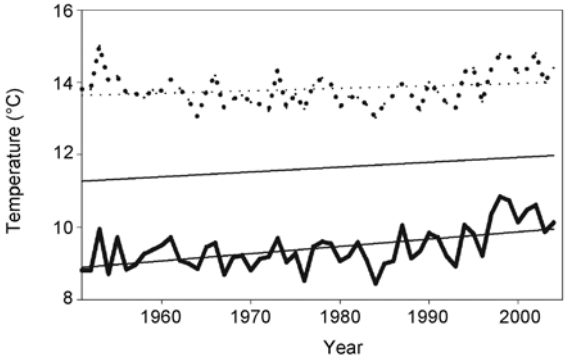


**Figure 12** The trends in the 54-year air temperature over regions north and south of the Qinling Mountains.

Figure 13 shows very weak decreasing trend in SMC on surface soil layer (1–10 cm), except for the small area on the north most Shaanxi. The trend coefficients in 30–50 cm soil layer range between 0.2 and 0.5 over the northern Shaanxi, suggesting that the SMC decreasing at a stronger rate compared to surface soil layer (1–10 cm) over middle and southern Shaanxi. The trend coefficients in 50–80 cm soil layer range between 0.2 and 0.6, and between 0.2 and 0.7 in 80–100 cm soil layer. The spatial distribution in trend coefficients suggested that the decreasing trend in soil moisture contents is strong in the northern boundary of Shaanxi, while weak decreasing trend appeared in most of the middle and southern Shaanxi. As the soil depth increases, the decreasing trend is stronger. The area of strong decreasing SMC also expands rapidly as the soil depth increases. The significant decreasing trend of soil moisture variations in deeper soil layer in the region north of the Qinling Mountains is primarily associated with the decreasing precipitation. Decreasing precipitation causes the declining in river flow or even causes the drying up (zero flow) in the river, thereby causing a low groundwater tables and drier soil. On the other hand, the increasing air temperature increases the soil evaporation and plant transportation, further decreasing the SMC in the soil. Further investigations are necessary to understand the detailed mechanism that caused the decreasing trend in soil moisture.

## 5 Discussion and conclusions

In this study, soil moisture in Shaanxi Province was simulated by SWAT for the period of 1951–2004 based on the data on DEM, soil types, soil properties, vegetation properties, land use types, and atmospheric *in situ* observations. Modeled soil moisture content was evaluated using the *in situ* observations of soil moisture in the region, and then compared to the soil moistures in NCEP/NCAR and ERA40 reanalyses. The results suggest that the SWAT can reasonably simulate the observed temporal variations and long-term trend in SMC. However, the model contains a large bias in simulating the long-term mean amount of SMC, partly because the definition of SMC in the model is different from the observations. The soil moisture simulated by SWAT is more consistent with the observations compared to the NCEP/NCAR and ERA40 reanalyses in terms of the linear trend and the amplitude of variation.

The simulated soil moisture in Shaanxi Province during 1951–2004 suggests that the soil moisture in surface soil layers is higher over the Baiyu, Qinling, and Daba moun-

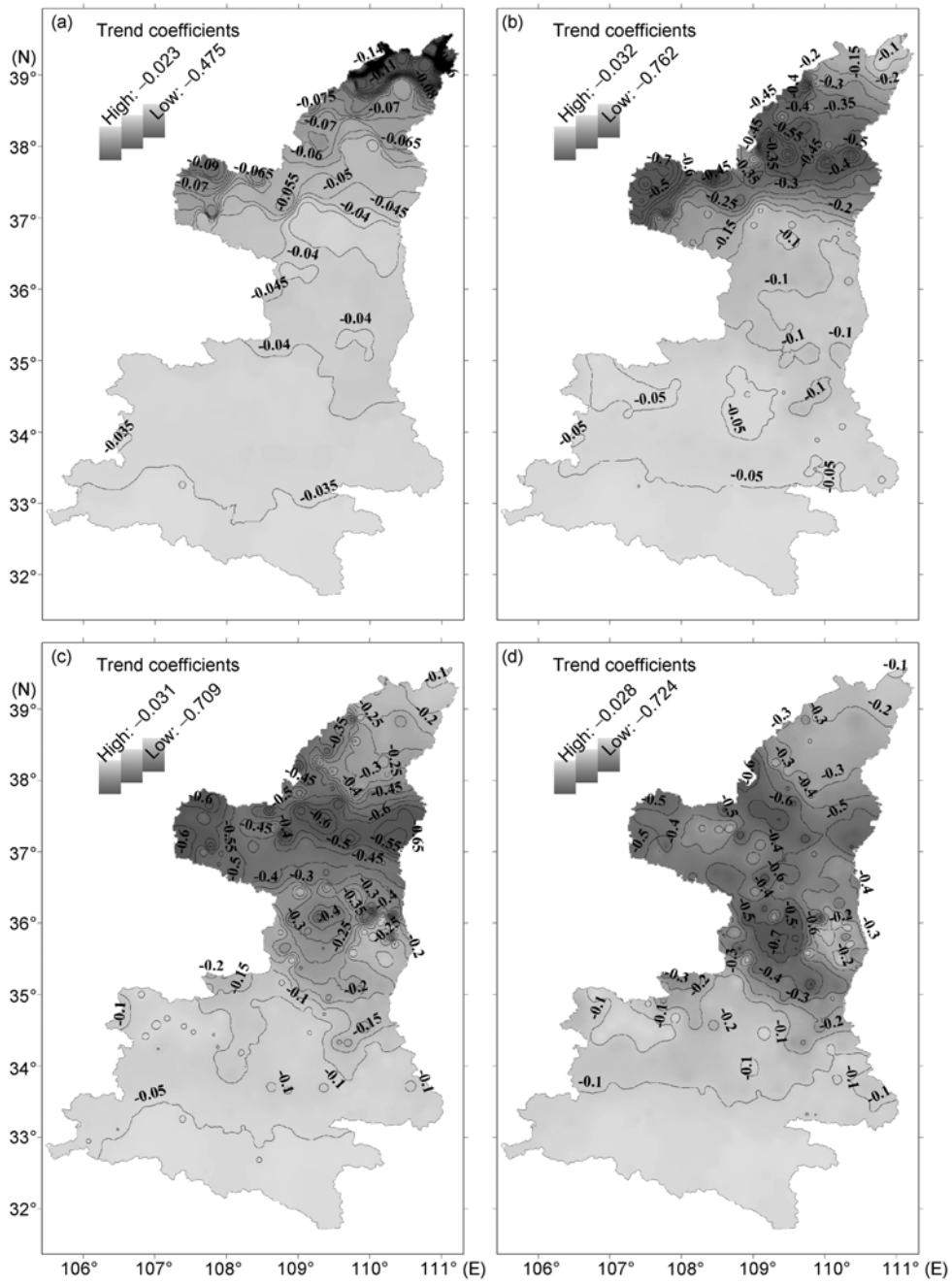


**Figure 13** Distribution patterns of trend coefficients in soil moisture variations. (a)–(d) indicate the trend coefficient variations in 1–10, 30–50, 50–80 and 80–100 cm soil layers respectively.

tainous zones, whereas in the deeper soil layers, soil moisture is higher in the Luouhe, Jinghe, and Weihe river basins. Soil moisture in various soil layers over 54-year period presents a generally decreasing trend. Downward trend in soil moisture is more significant in region north of the Qinling Mountains than the south. The variability in soil moisture simulated by SWAT generally responds to precipitation decreasing and temperature rising in the region. Following the accelerated decreasing in precipitation and rising in surface temperature since 1980, the soil moisture is decreasing rapidly.

The hydrological models are usually applied to investigate the hydrological processes in a river basin. In this study, due to very limited observations, the area of interest is selected over the Shaanxi Province, which could cause some tributary flows intercepted around the study area, which likely will introduce some artificial errors. Such errors could be very small as the focus of this study is principally on soil moisture variability, not the river flow. Previous studies suggested that the SWAT is able to evaluate the an-

thropogenic influence on soil moisture variability, which was not considered in this study due to insufficient *in situ* observations. The influence of human on the soil moisture certainly deserves further study.

In summary, SWAT can reasonably simulate the spatio-temporal variations and trend of regional soil moisture, particularly on shallow soil layers. Therefore, the SWAT may become a good tool to study the regional hydrological variations and the interactions between the land and atmosphere.

*This work was supported by Key Program of National Natural Science Foundation of China (Grant No. 40830956), Major State Basic Research Development Program of China (Grant No. 2006CB400504) and National Natural Science Foundation of China (Grant Nos. 40775055, 40828004). The authors thank all peer-reviewers for their valuable comments in revising this paper.*

1 Ma Z G, Fu C B, Xie L, et al. Some problems in the study on the relationship between soil moisture and climate change (in Chinese). Adv Earth Sci, 2001, 16: 563–568
2 Sun S F. Physical, Biochemical and Parameterized Models on Land Processes (in Chinese). Beijing: China Meteorological Press, 2005
3 Kalnay E, Kanamitsu M, Kistler R, et al. The Ncep/Ncar 40-year reanalysis project. Bull Amer Meteorol Soc, 1996, 77: 437–471
4 Uppala S M, Kållberg P W, Simmons A J. The Era-40 re-analysis. Quart J R Meteorol Soc, 2005, 131: 2961–3012
5 Vinnikov K Y, Robock A, Speranskaya N A. Scales of temporal and spatial variability of midlatitude soil moisture. J Geophys Res, 1996, 101(D3): 7163–7174
6 Li H B, Robock A, Liu S X, et al. Evaluation of reanalysis soil moisture simulation using updated Chinese soil moistrue observations. J Hydrometeorol, 2005, 6: 180–193
7 Ma Z G, Fu C B. Decadal variations of arid and semi-arid boundary in China (in Chinese). Chin J Geophys, 2005, 48: 519–525
8 Zuo Z Y. Influence of soil moisture anomaly in east China on the East Asian Summer Monsoon (in Chinese). Doctoral Dissertation. Beijing: Graduate University of Chinese Academy of Sciences, 2007
9 Zhang W J. Spatial distribution and temporal variation of the observed and simulated soil moisture over China (in Chinese). Masteral Thesis. Beijing: Graduate University of Chinese Academy of Sciences, 2006
10 Abbott M B, Bathurs J C, Cunge J A, et al. An introduction to the European hydrological system—System Hydrological European, "SHE", I: History and philocally-based distributed modelling system. J Hydrol, 1986, 87: 45–59
11 Sugawara M. Tank model. In: Singh V P, ed. Computer Models of Watersheld Hydrology. Littleton, Colo: Water Resources Publications, 1995
12 Beven K J, Lamb R, Romannowicz P, et al. Topmodel. In: Singh V P, ed. Computer Models of Watersheld Hydrology. Littleton, Colo: Water Resources Publications, 1995
13 Bosch D D, Sheridan J M, Batten H L, et al. Evaluation of the SWAT model on a coastal plain agricultural watershed. Trans Am Soc Agr Eng, 2004, 47: 1493–1506
14 Zhao R J, Liu X R. The Xin'anjiang Model. In: Singh V P, ed. Computer Models of Watersheld Hydrology. Littleton, Colo: Water Resources Publications, 1995
15 Jia Y W, Ni G H, Kawahara Y, et al. Development of WEP Model and its application to an urban watershed. Hydrol Process, 2001, 15: 2175–2194
16 Wang L, Wang Z J, Lin H, et al. A distributed hydrological model-GBHNM and its application in middle-scale catchment (in Chinese). J Glaciol Geocryol, 2006, 28: 256–261
17 Dickinson R E, Hendersonsellers A, Rosenzweig C, et al. Evapotranspiration models with canopy resistance for use in climate models—A review. Agric For Meteorol, 1991, 54: 373–388
18 Sellers P J, Mintz Y, Sud Y C. The Design of a simple biosphere model (SiB) for use within general circulation models. J Atmos Sci, 1986, 43: 505–531
19 Sellers P J, Randall D A, Collatz G J, et al. A revised land surface parameterization (SiB2) for atmospheric GCMs. 1. Model formulation. J Clim, 1996, 9: 676–705
20 Sellers P J, Los S O, Tucker C J, et al. A revised land surface parameterization (SiB2) for atmospheric GCMs. 2. The generation of global fields of terrestrial biophysical parameters from satellite data. J Clim, 1996, 9: 706–737
21 Bonan G B. Comparison of 2 land-surface process models using prescribed forcings. J Geophys Res-Atmos, 1994, 99(D12): 25803–25818
22 Ji J J. A climate-vegetation interaction model: Simulating physical and biological processes at the surface. J Biogeogr, 1995, 22: 445–451
23 Stamm J F, Wood E F, Lettenmaier D P. Sensitivity of a Gcm simulation of global climate to the representation of land-surface hydrology. J Clim, 1994, 7: 1218–1239
24 Dickinson R E, Oleson K W, Bonan G, et al. The community land model and its climate statistics as a component of the community climate system model. J Clim, 2006, 19: 2302–2324
25 Niu G Y, Yang Z L, Dickinson R E, et al. A simple topmodel-based runoff parameterization (SIMTOP) for use in global climate models. J Geophys Res-Atmospheres, 2005, 110: D21106: doi: 10.1029/2005jd006111
26 Manabe S. Climate and the ocean circulation 1: The atmospheric circulation and the hydrology of the earth surface. Month Weath Rev, 1969, 97: 739–774
27 Yeh T C, Wetherld R T, Manabe S. The effect of soil moisture on the short-term climate and hydrology change—A numerical experiment. Month Weath Rev, 1984, 11: 474–490
28 Wang W Q. Numerical experiments of the soil temperature and moisture anomalies' effects on the short term climate (in Chinese). Chin J Atmos Sci, 1991, 15: 115–123
29 Dai Y J. The land surface model and application coupled with atmospheric cycle model (in Chinese). Doctoral Dissertation. Beijing: Graduate University of Chinese Academy of Sciences, 1995
30 Xie Z H, Yuan F, Duan Q Y. Regional parameter estimation of the VIC land surface model: Methodology and application to river basins in China. J Hydrometeorol, 2007, 8: 447–468
31 Arnold J G, Fohrer N. SWAT2000: Current capabilities and research opportunities in applied watershed modelling. Hydrol Process, 2005, 19: 563–572
32 Arnold J G, Srinivasan R, Muttiah R S, et al. Large area hydrologic modeling and assessment—Part 1: Model development. J Am Water Resour As, 1998, 34: 73–89
33 King K W, Arnold J G, Bingner R L. Comparison of green-ampt and curve number methods on Goodwin creek watershed using SWAT. Trans ASAE, 1999, 42: 919–925
34 Srinivasan R, Ramanarayanan T S, Arnold J G, et al. Large area hydrologic modeling and assessment—Part II: Model application. J Am Water Resour As, 1998, 34: 91–101
35 Arnold J G, Williams J R. Validation of SWRRB-simulator of waters in rural basins. J Water Res Planning Manage-ASCE, 1987, 113:

243–246
36 Knisel W G, Moffitt D C, Dumper T A. Representing seasonally frozen soil with the creams model. Trans ASAE, 1985, 28: 1487–1493
37 Leonard R A, Knisel W G, Still D A. Gleams: Groundwater loading effects of agricultural management systems. Trans Amer Soc Agri Engrs, 1987, 30: 1403–1418
38 Izaurralde R C, Williams J R, Mcgill W B, et al. Simulating soil C dynamics with epic: Model description and testing against long-term data. Ecol Model, 2006, 192: 362–384
39 Neitsch S L, Arnold J G, Kiniry J R, et al. SWAT2005 Theoretical Documentation, Version 2005. 2005
40 Geleyn J F, Preub H J. A new data set of satellite-derived surface albedo values for operational use at ECMWF. Arch Met Geoph Biocl Ser A, 1983, 32: 353–359
41 Zhang Q, Qian Y F. Monthly mean surface albedo estimated from NCEP/NCAR reanalysis radiation data (in Chinese). J Geogr Sci, 1999, 54: 309–317
42 Govaerts Y M, Lattanzio A, Taberner M, et al. Generating global surface albedo products from multiple geostationary satellites. Remote Sens Environ, 2008, 112: 2804–2816
43 Wischmeier W H, Johnson C B, Cross B V. A soil erodibility nomograph for farmland and construction sites. J Soil Water Conserv, 1971, 26: 189–193
44 Neitsch S L, Arnold J G, Kiniry J R, et al. Soil and Water Assessment Tool User's Manual, Version 2000. 2002, 125–136, 232–235